Atmospheric Environment 43 (2009) 2981–2996

Contents lists available at ScienceDirect

Atmospheric Environment

journal homepage: www.elsevier.com/locate/atmosenv

Flow and dispersion in street intersections

L. Soulhac [a], V. Garbero [b,c], P. Salizzoni [a,d,*], P. Mejean [a], R.J. Perkins [a]

[a] Laboratoire de Mécanique des Fluides et d'Acoustique, Université de Lyon, CNRS, Ecole Centrale de Lyon, INSA Lyon, Université Claude Bernard Lyon I, 36, avenue Guy de Collongue, 69134 Ecully, France
[b] Dipartimento di Matematica, Politecnico di Torino, Corso Duca degli Abruzzi, 24, 10129 Torino, Italy
[c] Golder Associates S.r.l., Via Banfo 43, 10155 Torino, Italy
[d] Dipartimento di Ingegneria Aeronautica e Spaziale, Politecnico di Torino, Corso Duca degli Abruzzi, 24, 10129 Torino, Italy

ARTICLE INFO

Article history:
Received 14 May 2008
Received in revised form
31 January 2009
Accepted 2 February 2009

Keywords:
Street canyon
Street intersection
Urban air pollution
Dispersion models

ABSTRACT

Street intersections play an important role in determining pollutant concentrations in the urban canopy – vehicle emissions often increase in the vicinity of road intersections, and the complex flow patterns that occur within the intersection determine the pollutant fluxes into adjoining streets and into the atmosphere. Operational models for urban air quality therefore need to take account of the particular characteristics of street intersections. We have performed an experimental and numerical investigation of flow and dispersion mechanisms within an urban intersection, and on the basis of our observations and results, we have developed a new operational model for pollutant exchanges in the intersection, which takes account of the non-uniformity of the pollutant fluxes entering and leaving the intersection. The intersection is created by two streets of square cross-section, crossing orthogonally; concentrations were measured by releasing a neutrally buoyant tracer gas from a line source located in one of the streets. As a general result, the numerical simulations agree well with the measurements made in the wind tunnel experiments, except for the case of ground-level concentrations, where the computed concentrations far from the axis of the line source are significantly lower than the measured values. In the first part of the study we investigate the influence of an intersection on the velocity and concentration fields in the adjoining streets; we show that the immediate influence of the intersection extends within the adjoining streets, to a distance of the order of the characteristic size of the streets. A large recirculating vortex is formed at the entrance to the cross-wind streets, and this determines the exchange of pollutants between the streets and the intersection. For some wind directions the average velocity in the street segment between intersections is the same as that which occurs in an infinitely long street with the same wind, but for other angles the average velocity in the finite-length street is significantly lower. The average concentration along a finite-length street is significantly different from that observed in an infinitely long street. In the second part of the study we investigate how the pollutant fluxes in the incoming streets are redistributed amongst the outgoing streets. An analysis of the mean streamlines shows that the flows remain relatively planar, with little variation over the vertical, and we have exploited this result to develop a simple operational model for the redistribution of pollutant fluxes within the intersection. This model has been further adapted to take account of the influence of fluctuations in wind direction over typical averaging periods. The resulting model is used in the street network model SIRANE.

1. Introduction

Street intersections play an important role in determining pollutant concentrations in the urban canopy. Firstly, traffic flows are disrupted, and vehicles are obliged to accelerate and decelerate, thereby increasing emissions. In congested intersections, or at intersections controlled by traffic lights, idling vehicles will increase emissions above the level for free-flowing traffic. Secondly, street intersections are regions where there is significant exchange of pollutants between the connected streets. So models of pollutant dispersion within the urban canopy need to take account of the specific effects induced by street intersections. And since pollutant concentrations are often measured close to, or within, street intersections, the correct analysis of these data requires a detailed understanding of the physical processes involved (Ott, 1977; Scaperdas and Colvile, 1999).

There have been several *in situ* experiments to investigate how traffic emissions vary in the vicinity of street intersections (O'Toole et al., 1975; Rosas et al., 1980; Bullin et al., 1982), and the results of

* Corresponding author at: Laboratoire de Mécanique des Fluides et d'Acoustique, Université de Lyon, CNRS, Ecole Centrale de Lyon, INSA Lyon, Université Claude Bernard Lyon I, 36, avenue Guy de Collongue, 69134 Ecully, France.
E-mail address: pietro.salizzoni@polito.it (P. Salizzoni).

1352-2310/$ – see front matter © 2009 Elsevier Ltd. All rights reserved.
doi:10.1016/j.atmosenv.2009.02.061

those studies have been used to develop semi-empirical models such as IMM and MICRO2, to estimate concentrations near crossroads (Benesh, 1978; Zamurs and Piracci, 1982; Griffin, 1983; Messina, 1983). But the experiments were performed in open areas (because the main interest was the influence of intersections on emissions, rather than on dispersion) and the models that have been developed do not explicitly consider the effects of the surrounding buildings, so they cannot reasonably be applied to the urban environment.

There have also been several studies of pollutant dispersion in urban street intersections using both experimental and numerical approaches. Hoydysh and Dabberdt (1994) and Hoydysh et al. (1995) carried out wind tunnel experiments for a grid of orthogonal streets, measuring concentrations of a tracer gas within the intersections. These studies demonstrated that the concentrations varied significantly within the intersection, with maximum values consistently located at street corners, and showed that the street aspect ratio had an important influence on conditions within the intersection. Robins et al. (2002) also performed wind tunnel experiments to investigate the dispersal of pollutants in an urban street intersection; their results showed that the flow was very sensitive to the wind direction relative to the intersection, so that even small asymmetries in the configuration could lead to very different dispersion patterns.

Numerical simulations of flow in street intersections have provided a detailed picture of some of the major flow mechanisms that occur. Hunter et al. (1990) studied the case of two streets crossing at right angles, and showed that when one of the streets was orthogonal to the wind direction, large vertical-axis recirculating regions formed in the cross-wind streets, at the interface with the streamwise street. In another study, Gadilhe et al. (1993) simulated the flow in a square in Nantes, analyzing the recirculating motions taking place within it. Scaperdas and Colvile (1999) studied the flow and the dispersion within a real intersection in London by means of field measurements and numerical simulations, focusing on the influence of the external wind on pollutant concentrations.

The flow field within and around a street intersection in London was measured as part of the DAPPLE project field campaign (Dobre et al., 2005); an analysis of those measurements showed that, at a short distance from the intersection, the main features of the flow in the streets were similar to those observed in idealised two-dimensional street canyons – a combination of flow channeled along the street, and a recirculating vortex with its axis parallel to the street axis. In this study, the streets that formed the intersection had a rather irregular geometry.

As far as we are aware, the only operational model for pollutant dispersion in urban street intersections was developed by Yamartino and Wiegand (1986). The model assumes that the pollutants in the intersection are well-mixed, so that the whole intersection can be treated as a single box containing pollutant with a uniform concentration, which is computed from a simple mass balance of the fluxes entering and leaving the box. Data from measurements and numerical simulations show that this is a rather unrealistic assumption, which limits the ability of the model to provide reasonable predictions of concentrations within the intersection and in the adjoining streets, so there is a need to develop a more realistic model, which can nevertheless be used in an operational context.

The various studies of flow and dispersion in urban street intersections all show that, even for simple configurations, the flow structure is very complicated, and a detailed description would require a large number of experiments and numerical simulations. An operational model must be able to treat an infinite variety of situations, rapidly, and with limited computing resources, so it will only be capable of reproducing some of the more basic aspects of mass and momentum exchange in the intersection. A reasonable objective for such an operational model, compatible with the conditions in which it is likely to be used, would be to compute the average concentration in the intersection and the average pollutant fluxes into and out of the adjoining streets, for given meteorological conditions and pollutant emissions. The average concentration is understood here to be taken over both space and time; the typical averaging period for an operational model would be of the order of 1 h, but in certain circumstances it could be as little as 15 min. The aim of the research presented here has been to understand the basic physical processes which determine mass and momentum exchanges between the streets that define the intersection, and to use the results of that work to develop a suitable operational model. The model that we have developed forms part of the urban dispersion model SIRANE, in which the urban canopy is modelled as a network of streets, with pollutant exchanges between different streets, and between the streets and the overlying atmosphere (see, for example, Fig. 1). In this model, each street segment is characterized by a constant height, width and direction, and street intersections are therefore defined as the nodes at which the street characteristics change. These nodes can be the junction of several different streets, but they can also be the points at which the height, width or direction of a street changes significantly. The model SIRANE has already been used to compute street level concentrations in several large European cities including Lyon, Paris, Grenoble, Turin and Milan (Soulhac et al., 2002, 2003, 2004; Boni et al., 2008; Biemmi and Gaveglio, 2007). More recently, the network approach was adopted by Hamlyn et al. (2007) to model pollutant dispersion within regular arrays of obstacles.

The geometry of real street intersections can be relatively complicated and a full description might require many parameters (the geometrical characteristic of the streets, the size and shape of the intersection, details of the roofs, building walls, ground…) so it seems unrealistic to attempt a universal classification of intersections. But many of these details are probably relatively unimportant in the average exchange of mass and momentum (Salizzoni et al., 2008). Firstly, the exchanges will be dominated by the faster moving parts of the flow, distant from the boundaries; secondly, temporal fluctuations in wind direction should smooth out some of the finer details, and the time average of the concentration fluxes should be less sensitive to individual details of the boundaries. By analogy with the representation of real streets as simplified canyons, a 'minimal' definition of a street intersection might therefore be the intersection of a number of simple, smooth-walled canyons, with a height equal to the average of the heights of the intersecting streets. This definition is also consistent with the context in which the operational intersection model is likely to be used, in which the contributing fluxes will be obtained from calculations based on the flow in individual street canyons.

In order to develop an operational model for the pollutant fluxes in a street intersection in an urban environment, we have investigated the simplest possible configuration, consisting of the orthogonal intersection of two identical streets, of square cross-section. Although simple and idealised, this configuration is nevertheless typical of a rather large number of street intersections in European cities. We have used both wind tunnel experiments and numerical simulations to study the velocity and concentration fields within the intersection, as a function of the external wind direction. The configuration is described in detail in Section 2, together with the experimental facilities and the numerical methods that have been used. We focus first (Section 3) on the velocity and concentration fields generated in one of the streets adjoining the intersection, to establish the 'zone of influence' of the intersection; the results from the street network study are compared with corresponding results for an isolated street of infinite length. Then, in Section 4, we investigate flow and dispersion within the core of the intersection as a function of the external

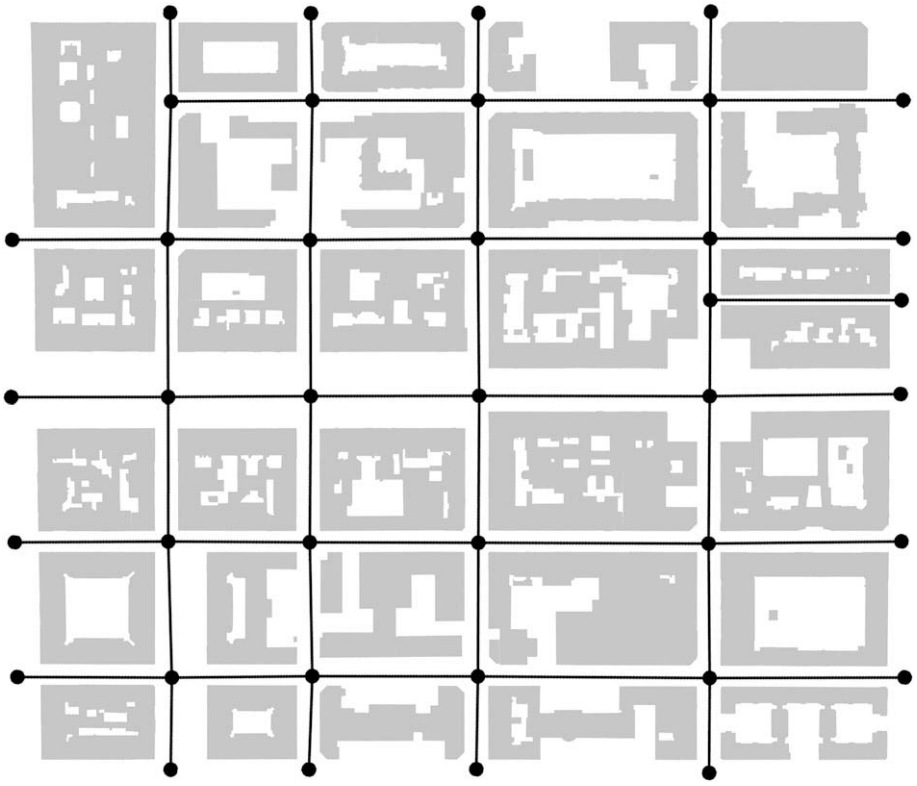

Fig. 1. The street network approach applied to a district of the city of Lyon (France).

wind direction. In particular, we focus on the topology of the flow in the intersection, so as to understand how the flows from the incoming streets mix and are redistributed amongst the outgoing streets. Finally, in Section 5, we present a new operational model for the pollutant exchange in a street intersection. This model can be integrated into urban dispersion models in order to improve the evaluation of the pollutant turbulent exchanges in street intersections, and forms part of the SIRANE urban dispersion model, developed at the Laboratoire de Mécanique des Fluides et d'Acoustique (LMFA), Ecole Centrale de Lyon.

2. Experimental and numerical methods

2.1. Wind tunnel experiments

The experiments were performed at the LMFA, in a recirculating atmospheric boundary layer wind tunnel, with a test section that measures 14 m × 2.5 m × 3.7 m.

A grid of streets was created by placing obstacles (10 cm high and 50 cm × 50 cm in plan) on the floor of the wind tunnel in a regular pattern, 10 cm apart, as illustrated in Fig. 2. This created streets with a square cross-section (height $H = 10$ cm, width $W = 10$ cm) and a length $L = 50$ cm. At a scale factor of 1:200 this would correspond to streets measuring 20 m × 20 m in cross-section.

The boundary layer was generated using a combination of Irwin spires at the entry to the test section, and roughness elements distributed randomly on the floor over a distance of about 6 m upwind of the measurement section. The incoming velocity profile in the boundary layer has a logarithmic form:

$$U = \frac{u^*}{\kappa} \ln\left[\frac{z-d}{z_0}\right] \quad (1)$$

with a displacement height d of 20 mm, a roughness length z_0 of 2.7 mm and a friction velocity u^* of 0.27 ms^{-1}. These values were obtained by fitting the assumed profile (Equation (1)) to the measured velocities, using the method described in Salizzoni et al. (2008).

In the analysis that follows, we will refer to the street parallel to the wind direction as street no. 1, and the street perpendicular to the wind as street no. 2, as shown in Fig. 2. This figure also defines the wind angle θ relative to the initial configuration $\theta = 0°$; experiments have been performed for $\theta = 0°$, 15°, 30°, 45°, 60°, 75° and 90°.

Velocities were measured using a two-component Laser Doppler Anemometry system. The dispersion of pollutant within a street intersection was investigated by placing a line source of pollutant (length $2L$) along the axis of street no. 1, as shown in Fig. 2. The source emitted a continuous mass flux Q of ethane (C_2H_6), which was chosen as a tracer gas because its molecular weight is nearly the same as that of the air. The tracer gas concentrations were measured with a Flame Ionisation Detector. The homogeneity of the emission from the line source was tested before starting the measurement campaign (Meroney et al., 1996).

2.2. Numerical simulations

The numerical simulations were performed using two codes – *FLUENT* and *MERCURE* (Carissimo et al., 1995), a three-dimensional numerical code which implements a finite difference method to solve the Reynolds-Averaged Navier–Stokes equations. A standard k–ε turbulence model was used in both cases. The computations were performed using a Cartesian grid with variable spacing; closest to the rigid boundaries the spacing was set equal to $H/40$, and it increased with distance from the boundary. The roughness lengths of the roof and sidewalls of the street were set equal to $H/400$. The geometrical symmetry of the obstacle array was used to

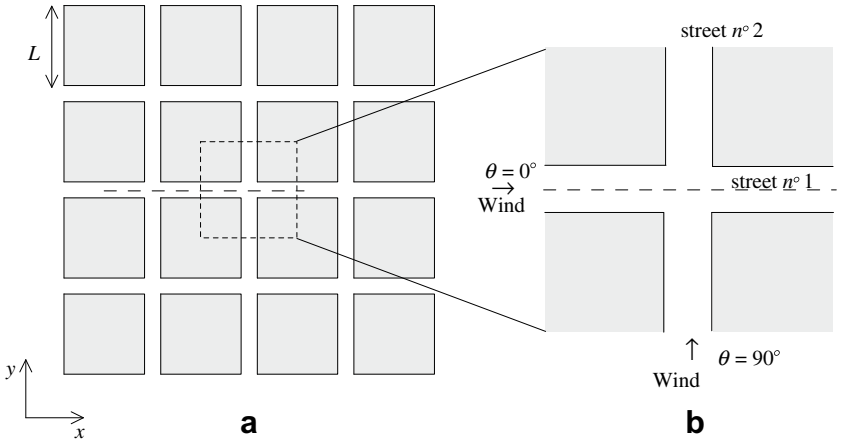

Fig. 2. Wind tunnel set up (on the left) and numerical domain (on the right); the dashed line represents the line source.

limit the size of the computational domain, and hence the computing time; the computations were performed for a single intersection, with periodic conditions on the inlet and outlet sections, so that the flow exiting from a street was identical to the flow entering the street at the upstream boundary. A condition of zero shear was applied at the upper boundary. Scaperdas and Colvile (1999) found that both symmetrical and asymmetrical numerical solutions were possible for a symmetrical geometry, like the one investigated here, and the use of periodic boundary conditions ought to permit asymmetrical solutions. However all the solutions we obtained were symmetrical, but we did not attempt to push the model towards asymmetrical solutions. Scaperdas and Colvile (1999) also found that concentration measurements in the side streets were not very repeatable, and this may be another indication of the possible coexistence of symmetrical and asymmetrical solutions. In this study the numerical model was used to compute steady state solutions, so this would also have the effect of selecting some solution – possibly the symmetrical ones – over unsteady, asymmetrical solutions.

3. Flow and dispersion in the streets connected to an intersection

Previous studies (Robins et al., 2002) have shown that the direction of the external wind can have an important influence on the flow within a street intersection, and on the transport and mixing of pollutants. We have therefore measured the velocities and concentrations in the streets forming an intersection, for different external wind directions; those configurations have also been simulated numerically. Because the obstacles in the array are arranged symmetrically, it is only necessary to study wind directions between 0° (wind parallel to the x-axis) and 45°, so these are the limiting cases for our analysis.

3.1. External wind perpendicular to the x-axis ($\theta = 90°$)

This configuration, illustrated in Fig. 3, represents one of the two limiting cases for the wind direction; the wind blows along-street no. 2 and perpendicularly across street no. 1, so that, sufficiently far from the intersection, we should expect the flow in the street no. 1 to resemble that in a classical street canyon, with a recirculating cell occupying most of the street. Since the wind blows parallel to street no. 2 the flow within the street should be relatively rectilinear, and this means that there must be a transition zone at the entrance to the street no. 2, in which the recirculating cell develops. This raises three interesting, and practically important questions:

- How does the flow adapt from rectilinear flow in street no. 2 to the recirculating cavity flow in street no. 1?
- What is the characteristic length of this transition zone?
- Does the transition have any important influence on the flow in street no. 2?

In order to understand how the transition takes place, we need to define the region of transition. To do this, we have measured horizontal and vertical velocities (u and w) within the street no. 1, along the horizontal and vertical planes passing through the centre of the cavity, at different distances (x) from the centre of the intersection. The measured velocities have been normalised by the external wind speed at roof height U_H and normalised profiles are plotted in Fig. 4 for five different distances from the intersection ($x/H = 0.6, 0.8, 1.4, 2.2, 3$); the length of the street no. 1 is equal to $5H$, so the profiles at $x/H = 3$ corresponds to flow close to the midpoint of the street, and by symmetry the conditions here should be closest to those in an infinitely long street with a perpendicular external wind.

On the same profiles we have also plotted the results of the corresponding 3-D numerical simulations and the velocity profiles measured in a previous wind tunnel study of flow and dispersion in an isolated street canyon, which corresponds to the case of an infinitely long street without end effects (Soulhac, 2000).

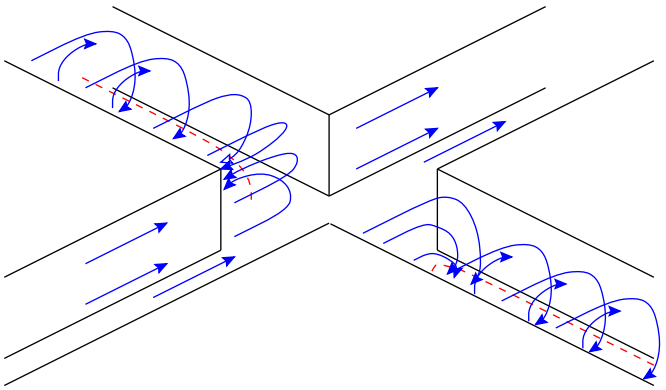

Fig. 3. Visualisation of the main structure of the flow in a street connected to an intersection (numerical simulation).

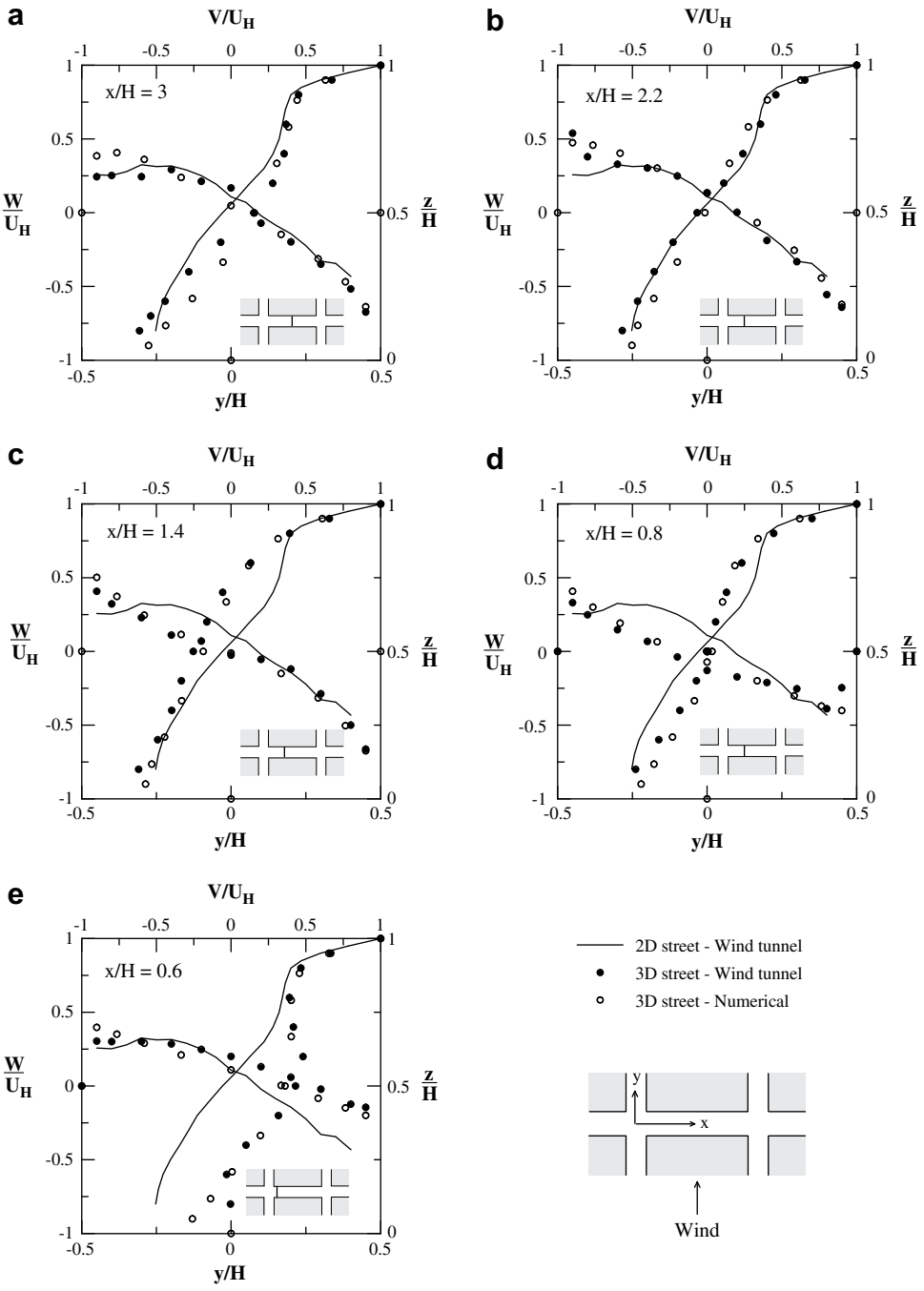

Fig. 4. Mean velocity profiles at different sections of the street no. 1: comparison between numerical and experimental results. a) $x/H = 3$; b) $x/H = 2.2$; c) $x/H = 1.4$; d) $x/H = 0.8$; e) $x/H = 0.6$.

The first point to note is that the numerical results agree well with the measured velocities, for all values of x/H, even close to the intersection, where the flow is likely to be highly three-dimensional. This means that we can use the numerical simulations to obtain additional information about flow in the transition zone that might be hard to extract from experimental measurements.

The second point is that all the profiles exhibit the characteristic form of a recirculating cell driven by an external flow, with a downward flow on the downwind face of the cavity, and an upward flow on the upwind face. The flow is driven by the shear from the external wind, and this is demonstrated by the steep gradient in the horizontal velocity, at the top of the cavity.

A comparison between the 3-D and the 2-D profiles shows that there is only one position ($x/H = 2.2$) where the two are in close agreement. As already argued, symmetry considerations suggest that the closest agreement ought to occur for $x/H = 3$ but this is clearly not the case. One possible explanation could be that the flow is very sensitive to wind direction, and that a small error in positioning the array or a small dis-symmetry in the array could lead to a large displacement of the 'neutral' profile along the street. But the agreement between numerical and experimental profiles, for both $x/H = 2.2$ and $x/H = 3$, suggests that this is not the case, for these small errors in alignment are not present in the numerical simulations.

On the basis of these measurements it would seem reasonable to conclude that the influence of the intersection penetrates into the street to a distance between 1.4H and 2.2H.

We can infer some aspects of the complicated 3-D structure of the flow in the transition region from the way in which the velocity profiles evolve with distance from the intersection, notably by comparing them with the profiles of infinitely long street. The basic flow pattern within the street remains that of a recirculating cell, filling the street, and driven by the wind above the street. Near the mid-point of the street the profiles for the 2-D and the 3-D street are similar, but there are some significant differences between the two, close to the intersection (e.g. $x/H = 0.6$). The downward velocities on the downwind face of the cavity are much lower in the 3-D street than in the 2-D street, indicating that less air must be entrained across the upper surface of the cavity. However at ground level the reverse flow, towards the upwind face of the cavity, is much greater in the 3-D street than in the 2-D street. Indeed, the upwind mass flux in the lower half of the street easily exceeds the downwards mass flux in the cavity on the downwind face. By conservation of mass, the upwind flux must be fed by the entrainment, at ground level, of air in the intersection, and this entrainment is driven by the vertical-axis recirculating region that forms at the entrance to the cross-wind street. This can be seen schematically in Fig. 3 – both the vertical-axis recirculation and the horizontal-axis recirculation contribute to an upwind flux at ground level in the cross-wind street, close to the intersection.

All along the cross-wind street (no. 1) the flow exhibits a rotating cell structure, with a centre that moves around as a function of distance from the intersection. This suggests that the flow has a helicoidal structure. The computational results agree well with the measured velocities, at all position in the cross-wind street, so the numerical model can be used to investigate some aspects of the flow that cannot be studied easily using experimental techniques.

In order to study the dispersion of pollutant along the cross-wind street (no. 1), and the exchanges that occur, both with the atmosphere and at the intersection, we placed a line source all the way along the centre of the cross-wind street, and across the intersection. Concentrations of tracer gas in the cross-wind street were measured at different distances from the intersection, and some of the profiles are shown in Fig. 5. The concentration field within the cross-wind street, on a plane perpendicular to the axis of the street, in the centre of the street ($x/H = 3$) is shown in Fig. 5a. The cavity is filled with a strong recirculating cell which transports the tracer from the line source at the bottom of the cavity – first upstream, then rising along the upwind wall before turning over at the top of the cavity. The concentration contours suggest that the centre of this recirculating cell is located at about half the cavity height, somewhat downwind of the axis of the street.

The vertical profile of dimensionless concentration at the mid-point of the street ($x/H = 3$) and on the street axis has been plotted in Fig. 5b, together with the corresponding profile obtained from numerical simulations, and an equivalent profile for an infinitely long street oriented perpendicular to the wind.

The measured and the computed profiles agree well over the full height of the cavity, but the concentrations are almost twice those measured in an infinitely long street. This means that the concentration distribution is still strongly affected by the finite length of the street. The velocity measurements show that the end conditions have no influence on the recirculating velocities at the mid-point of the cross-wind street, so the only possible explanation for the large difference in the concentration measurements is that there must be a significant component of the wind along the street, induced by the end conditions. The horizontal profile of concentration at mid-height (Fig. 5c) confirms that the computational results agree well with the measured data, and that once again the concentrations in a street of finite length are greater than those in an infinitely long street, by a factor that varies between 1.5 and 2. The profiles all show a double peak superimposed on a concentration that decreases with increasing distance downwind. The double peak arises from the way in which the recirculating cell transports the tracer gas around the cavity, from the source at ground level, and the general underlying decrease in concentration is due to the escape of tracer gas into the atmosphere, across the upper boundary of the cavity.

The overall increase in concentration in the finite-length street, compared with an infinitely long street, suggests that the end conditions might generate a flow along the street, from the intersection to the mid-point, which would transport pollutant along the street; continuity and symmetry conditions would then ensure that the pollutant left the street at the mid-point. To test this hypothesis we have plotted the measured and computed concentration profiles on the axes of the cross-wind street, at mid-height (Fig. 5d). Once again the numerical results agree reasonably well with the measured concentrations and provide at least partial confirmation of this hypothesis. There is a clear peak in the concentration at the mid-point of the cross-wind street, and the concentration decays symmetrically from this towards the ends of the street. The numerical simulations and the measurements agree reasonably well in their estimates of the peak concentration at the centre of the street.

Both the computed and the numerical profiles show that the rate at which the concentration decays along the street decreases towards the end of the street; the computed profile shows a clear minimum (at $x/H = 1.5$ and $x/H = 4.5$), followed by an increase in concentration, up to a value only slightly less than the peak value at the mid-point of the street. The measured profiles also show a slight peak in the concentrations at these points, but the peak concentrations are much lower than those computed in the simulations. This rather striking 'triple peak' concentration distribution occurs in both the experimental and the numerical results, and can only be explained by the rather complex three-dimensional structure of the flow in the street. The concentrations plotted in Fig. 5d are measured at the centre of the street, at the half height, and are not therefore necessarily representative of the cross-sectionally averaged concentration at the same position. The basic flow structure in the street consists of a single vortex (as shown in Fig. 5a) centred on the axis of the street, and driven by the external wind, so that the pollutant at the bottom of the cavity is transported towards the upwind face of the street. In an infinitely long street this structure is relatively stable, and will generate a constant concentration at the centre of the street, independent of the axial location. But in the configuration studied here, the basic configuration is perturbed by the flow structures that develop at each end of the street. These are essentially regions of recirculating flow, about a vertical axis, which entrain unpolluted air from the street aligned with the wind (street no. 1 in our configuration); the axis of this recirculating flow bends over at the top of the cavity, and becomes aligned with the axis of the street, so that the vertical-axis recirculating region blends into the larger horizontal-axis recirculating flow that occupies the large central part of the street. This is illustrated schematically in Fig. 3, and in more detail in Fig. 13c which shows the pathlines of pollutant particles emitted by a line source along the floor of the cavity, as computed in the numerical simulations. These pathlines, together with the concentration field at street level, largely explain the measured and computed concentration distributions along the axis of the street. In the vertical-axis recirculating region, the pollutant emitted by the ground-level line source is well-mixed at ground level throughout the recirculating region, and slowly lifted by the flow as it spirals upwards around the vertical axis. The peak in the concentration

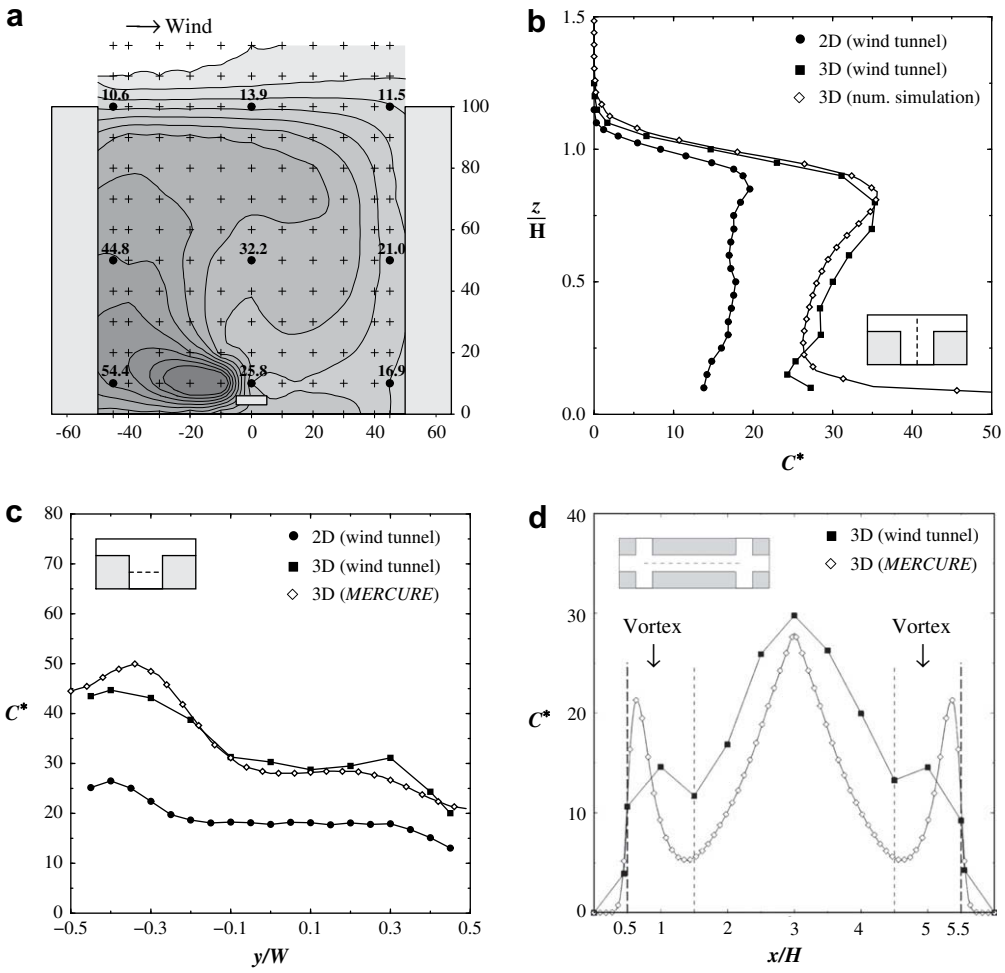

Fig. 5. Comparison between the concentration fields within an infinite street and within a street of finite length, for wind incident at an angle of 90°. a) Concentration field in the street no. 1 at $x/H = 3$ (wind tunnel). The crosses represent the measurement points. b) Vertical profiles of concentration $C^* = CU_HWL/Q$ at $y/W = 0$ and $x/H = 3$. c) Horizontal profile of concentration $C^* = CU_HWL/Q$ at $x/H = 3$ and $z/H = 0.5$. d) Horizontal profile of concentration $C^* = CU_HWL/Q$ at $y/W = 0$ and $z/H = 0.5$.

distribution at the end of the street is more or less coincident with the vertical axis of the recirculating region; the concentration falls off very rapidly towards the open end of the street, because of the rapid flow of non-polluted air in the street aligned with the wind. On the other side of the recirculating region the polluted air leaves the region at the upper surface of the cavity, and on the upwind side of the cavity, because it is then carried across the top of the cavity by the external wind. This means that the reverse flow at the bottom of the cavity is essentially provided by clean air entrained from the street aligned with the wind, and explains why the concentration on the street axis drops to a minimum on the inside edge of the recirculating region. This entrained air will provide a steady drift along the street, towards the mid-point of the street, converting the 2-D recirculating flow of the infinite street into a helical motion, with an angle of inclination that varies with position over the cross-section of the street; the recirculating flow is slowest at the bottom of the cavity – so the angle of inclination (of the pathlines) relative to the external wind direction is greatest there – and fastest at the top of the cavity, where the pathlines are more or less aligned with the external flow. As a result the projection of the pathlines onto a horizontal plane resembles a sawtooth wave along the axis of the street, as can be seen in Fig. 13c. If the street and the line source were infinitely long, these effects on their own would still not be sufficient to explain the observed concentration variation along the axis of the street – the simplest way to see this is to imagine the line source emitting a constant stream of particles, without any diffusion; the particle pathlines would then form a sheet wrapped around the centre of the main recirculating cell, and the conditions in any cross-section of the street would be identical, independent of the axial location of the cross-section. But in the finite-length street the surface composed of the particle pathlines wrapped around the centre of the street now contains a band – a helix of finite width, corresponding to the clean air entrained at the end of the street. If the particle paths were centred on the axis of the street, and if diffusive effects were the same throughout the cross-section, this still would not be sufficient to generate an axial variation in centreline concentration. But in fact the recirculating cell is not centred on the axis of the street, as the velocity profiles (Fig. 6a–e) show, and so as the clean air winds its way down the street the distance of the plume centreline from the centre of the street varies, and it is this meandering that gives rise to the axial variation in concentration on the street centreline. A corollary of these hypotheses is that if the experiment were to be repeated with a very much longer street, the vertical-axis recirculating cell should not change very much – because it is determined principally by conditions at the entrance – but additional peaks in the centreline concentration should occur on each side of the mid-point of the street, corresponding to additional 'turns' in the helix. The computed concentration agree reasonably well with the measured values, except close to the ends

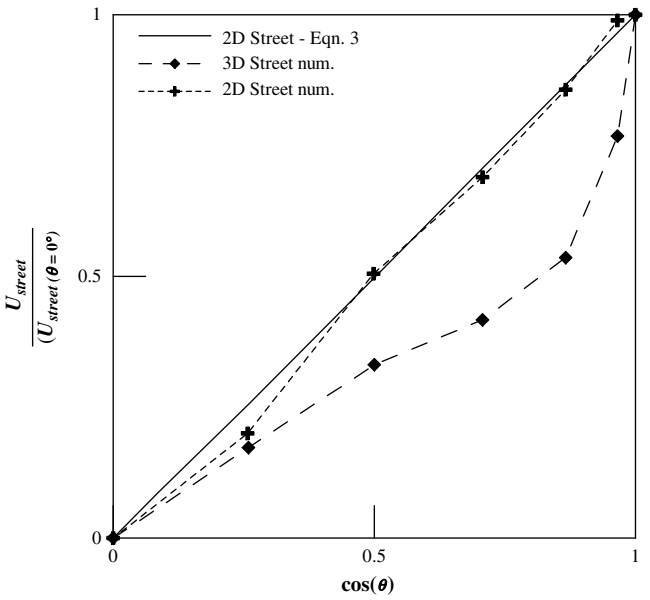

Fig. 6. Mean velocity within a street: comparison between a 2-D street and a 3-D street.

of the streets, where the numerical values significantly exceed the measured ones. This is probably because the line source is represented in the calculations as infinitely thin, whereas in the experiments the line source emits over a finite width. So there is an initial dilution of pollutant, close to the source, which is absent from the numerical simulations. Consequently, the numerical simulations will tend to underestimate the dispersion and overestimate the concentrations close to the source.

3.2. Influence of the external wind direction

Previous studies (Soulhac et al., 2008; Dobre et al., 2005) have shown that in the general case of wind incident on the street at any angle, the flow in the street is helicoidal, provided that the street is long enough. This flow pattern arises from the superposition of the along-street and cross-street components, and this decomposition was exploited by Soulhac et al. (2008) to develop a simple model for the spatially averaged flow along the street.

If we consider a wind which blows above the street with speed U, at an angle θ, then the velocity induced within the street and parallel to it, can be denoted $U_{\|}$. This velocity varies throughout the volume of the street, but the street-averaged value can be defined as

$$U_{street} = \frac{1}{HW}\int_0^W \int_0^H U_{\|}(y,z)dydz \tag{2}$$

Soulhac et al. (2008) then showed that for a given external wind velocity U, blowing at an angle θ to the street axis, the mean velocity along an infinite street is modelled reasonably well by the mean wind speed resolved parallel to the street:

$$U_{street}(\theta) = U_{street}(\theta = 0^\circ)\cos(\theta) \tag{3}$$

This is not the case for a street of finite length and the end effects caused by the intersections could modify the simple theoretical relationship for an infinitely long street (Equation (3)). To test this we have calculated the street-averaged velocity, for a finite-length street, and for different incidence angles, and the results are plotted in Fig. 6, together with the result for the simple model for an infinite street. This shows that the simple model agrees well with the computed average velocities for an infinitely long street, but that it tends to overestimate the velocities for a street of finite length. This overestimate is proportionally greatest for wind angles of 45° and 60°, but this is also very sensitive to wind direction when the angle is close to zero; this is probably the result of flow entrainment into the side streets by the vertical-axis recirculating region that forms at the entrance to the side street. The side street downwind of the intersection will entrain a significant quantity of air, thus reducing the average velocity in the main street. The weak component of the wind along the side street will help transport flow away from the intersection. On the opposite side of the intersection, a similar recirculating region forms for very low angles of incident wind, and this will also entrain fluid out of the main street, as well as tending to inhibit flow from the side street entering the main street. The net effect is therefore to remove momentum from the flow along the main street and it is only when the wind is perfectly aligned with the main street that this effect disappears. This effect is likely to be very sensitive to the geometry of the street – the extent of the recirculating regions will depend on the aspect ratio of the streets, for example – so the case of a wind exactly aligned with the main street may be a very special case which hardly ever occurs in practice. This would imply that even at a wind angle of 0°, the mean flow in a street with intersections will be substantially less than the value computed for an infinitely long street without intersections.

4. Flow and dispersion within a street intersection

In this section we investigate how the flow in a street intersection redistributes pollutant amongst the adjoining streets, and how this depends on the wind direction. To begin with we consider the basic case in which the wind is parallel to one of the streets – street no. 1, in which we have placed a line source of pollutant – and then we investigate the influence of wind direction; in total, we have examined 7 different angles (0°, 15°, 30°, 45°, 60°, 75° and 90°).

We are particularly interested in the exchanges between the different streets, and we can obtain some indication of these by examining the streamlines of the flow entering from different streets, as shown, for example, in Fig. 7b.

4.1. Wind parallel to the street ($\theta = 0^\circ$)

The graph of the velocity vectors at half height ($z = H/2$) plotted in Fig. 7a shows that several effects influence the velocity field within the intersection. Firstly, the flow separation at the upstream corners of the side streets leads to the formation of vertical-axis recirculating zones at the entrances to the two side streets, which penetrate into the side streets a distance of the order of the street width. These recirculating zones also appear to extend a small way into the main street – probably the result of the growth of the shear layer which forms downstream of the flow separation. The graph of the mean streamlines in the street (Fig. 7b) shows that the vertical-axis vortices in the two side streets are principally responsible for the exchanges between the streets; those exchanges are essentially limited to the fluid exiting closest to the sidewalls. There is very little flow from the side street into the main street (no. 1) so, by conservation of flux, the flow in the main street must entrain air from the overlying canopy, whilst some of the flow in the side streets must leave through the top surface, into the overlying canopy. In terms of pollutant dispersal, this means that polluted air from street no. 1 must be entrained into the side streets before being vented to the atmosphere, further along the side street. The net effect of this is that the intersection generates an enhanced lateral diffusion of pollutant into the overlying atmosphere.

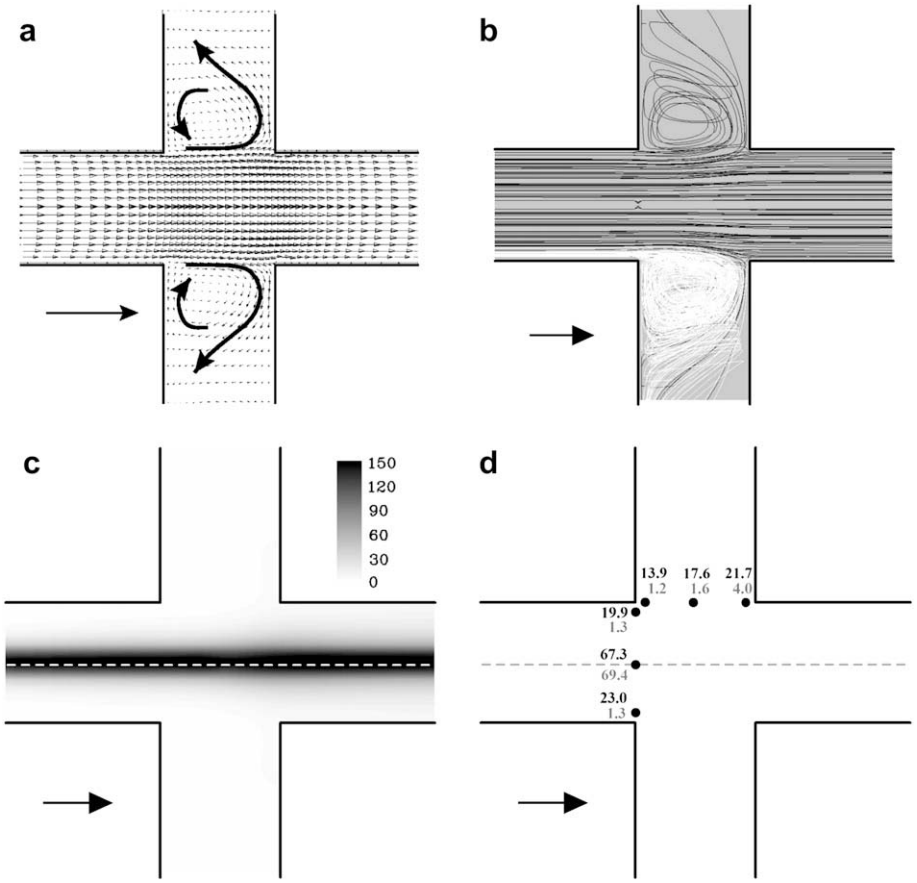

Fig. 7. Flow and dispersion in a street intersection for $\theta = 0°$. a) Velocity field at $z = H/2$. b) Streamlines crossing the end of the street no. 1 (black) and streamlines crossing the end of the street no. 2 (white). c) Concentration field C^* on the ground in case of a line source placed in the street no. 2 (MERCURE). d) Concentration values on the ground: comparison between wind tunnel measurements (black) and MERCURE simulations (grey).

Fig. 7 also shows that the streamlines in the main street remain fairly uniform with height; the image is a projection of a large number of streamlines at different heights, and there are very few that cross each other. This is far from true in the side street, where the flow is strongly three-dimensional. The plot of ground-level concentrations (Fig. 7c) shows that the mixing in the main street is strongly enhanced downstream of the intersection. Fig. 7d shows a quantitative comparison of the measured and computed concentrations at selected points around the intersection. The numerical model and the measurements agree well on the axis of the main street, but are substantially different at all other points along the centreline; the numerical model consistently underestimates the measured concentrations, by factor between 5 and 20. This difference can be explained by fact that the velocity and concentration fields are very sensitive to small asymmetries in the intersection (see, for example, Robins et al., 2002) so that even a slight displacement of the plume centreline can lead to significant differences in concentrations at a given location.

4.2. The influence of wind direction

In order to investigate the influence of wind direction we have repeated the preceding measurements and analysis for wind directions of 15°, 30°, 45°, 60°, 75° and 90°. The corresponding results for those cases are presented in Figs. 8–13.

The graphs of velocity vectors (Figs. 8a–13a) and streamlines (Figs. 8b–13b) show that as the direction turns ($\theta = 15°$), the recirculating zone in the 'upwind' side street rapidly leaves the side street, and reforms in the main street, downwind of the intersection. The upwind corner of the intersection remains a separation point, but because there is now a component of flow along the side street, directed towards the intersection, the flow leaks out into the mainstream, and there is no recirculation region at the end of the side street. The downwind corner of the intersection also becomes a separation point – because the flow from the side street cannot turn immediately through 90° – and so a recirculation region is established there. Once the wind angle reaches 45° the flow pattern in the intersection becomes symmetrical about the diagonal, with identical recirculating regions in the two downstream streets (Fig. 10a and b). As the wind direction increases from 45° to 90°, the flow patterns simply become rotated and reflected versions of those obtained for the complementary angles ($90° - \theta$), since the streets and the obstacles are all symmetrical.

It is important to note that in all these cases, there is very little evidence of time-averaged streamlines crossing within the intersection which means that the direction of the time-averaged velocity within the intersection varies little with distance from the ground. This suggests that the average flow within the intersection can be considered essentially two-dimensional, i.e. independent of distance from the ground. Similar results were obtained in the wind tunnel measurements of Kastner-Klain and Plate (1998) and in the wind tunnel simulations of the Dapple site by Carpentieri (2006). We will exploit these results later to propose a simple model for flux distribution in the intersection.

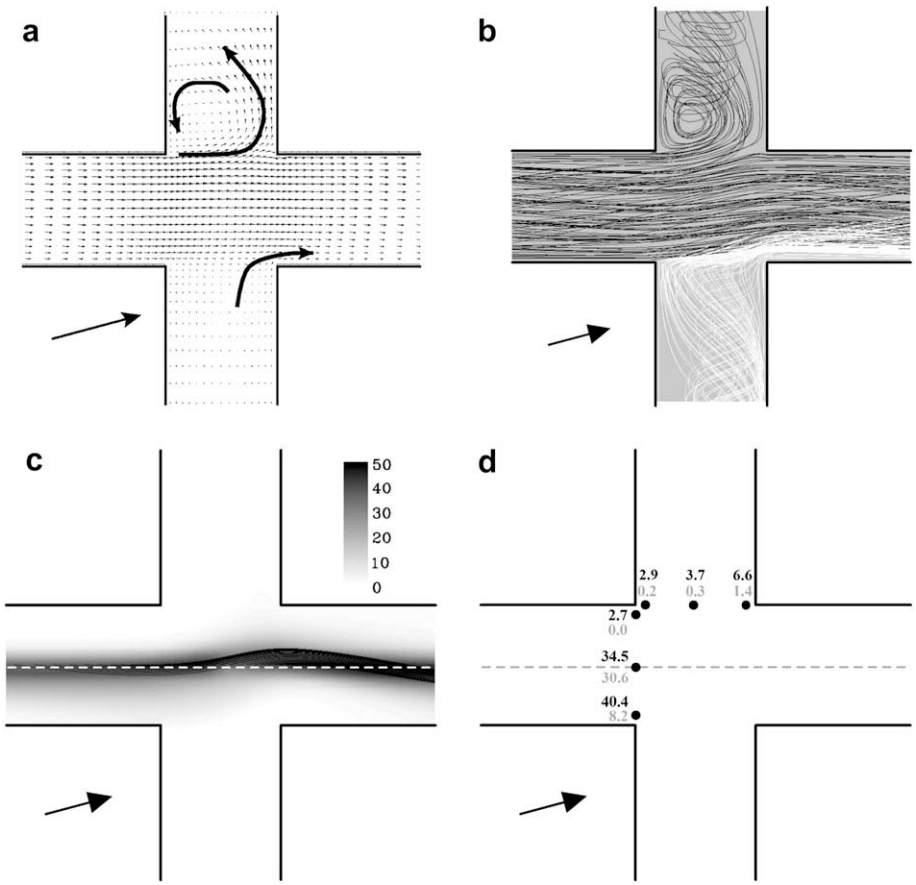

Fig. 8. Flow and dispersion in a street intersection for $\theta = 15°$. a) Velocity field at $z = H/2$. b) Streamlines crossing the end of the street no. 1 (black) and streamlines crossing the end of the street no. 2 (white). c) Concentration field C^* on the ground in case of a line source placed in the street no. 2 (MERCURE). d) Concentration values on the ground: comparison between wind tunnel measurements (black) and MERCURE simulations (grey).

The graphs of the concentration at ground level (Figs. 8c–13c and 8d–13d) show that there is very little diffusive transport of pollutant into the side streets. Upstream of the intersection the change in wind direction immediately generates an asymmetric concentration distribution in the main street, as the recirculating flow in the street carries ground-level pollutants upstream. For $\theta = 15°$, 30° (Figs. 8c–11c) the influx from the side street immediately deflects the ground-level pollutants to the downwind side of the street – overcoming the recirculating flow in the street – but the deflection is not enough to push the pollutants into the side street. At 45° the peak in the concentration is deflected sufficiently that it impacts on the downstream corner, with half the pollutants going into the side street, and half remaining in the main street. The recirculating patterns in the main street downwind of the intersection are rather complicated – the external wind creates large-scale recirculating flows in the street, with a horizontal axis, generating a helical type flow (Soulhac et al., 2008; Dobre et al., 2005), whilst the separation from the downwind corner generates a smaller localised recirculating region, with a vertical axis. The interaction of these recirculating flows ensures that the pollutant is rapidly mixed across the whole of the main street, downwind of the intersection.

The quantitative comparisons of measured and computed ground-level concentrations (Figs. 8d–13d) show the same general trend as for the case $\theta = 0°$; the numerical model computes peak centreline concentrations that are close to the experimental values for all wind directions, but greatly underestimates the off-centre concentrations in all cases. The higher ground-level concentration at the street corners observed in the experiments can be again explained by the effect of the initial dilution associated with the finite width of the line source, compared with the infinitely thin line source which is assumed in the numerical model.

Both the measured and the computed concentrations show that local average concentrations vary within the intersection. This suggests that the instantaneous variation in concentration will be even greater, due both to fluctuations in the overall concentrations and fluctuations in the wind direction, which will displace the entire concentration field (Hoydysh and Dabberdt, 1994). The consequences of this are discussed further in Section 5.3.1.

5. A simple model for the dispersion of pollutants in a street intersection

The experimental and numerical study of flow and dispersion in an intersection has shown that the physical processes involved are complex and depend on a wide variety of parameters. Even fully 3-D calculations such as those presented in Section 4 cannot reproduce all of the details, and are far too time-consuming to be used for practical operational modelling. But, as various studies have shown, street intersections play an important role in the redistribution of pollutants between streets, and in the exchanges between streets and the atmosphere, so their influence has to be included in operational urban air-quality models.

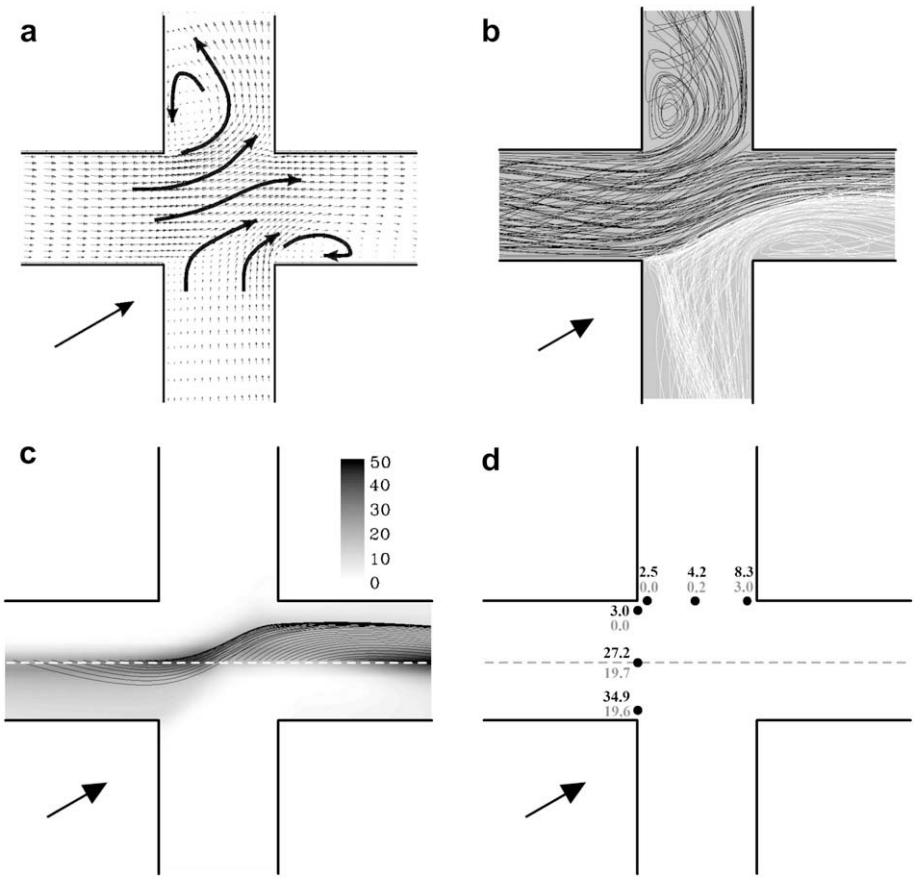

Fig. 9. Flow and dispersion in a street intersection for $\theta = 30°$. a) Velocity field at $z = H/2$. b) Streamlines crossing the end of the street no. 1 (black) and streamlines crossing the end of the street no. 2 (white). c) Concentration field C^* on the ground in case of a line source placed in the street no. 2 (MERCURE). d) Concentration values on the ground: comparison between wind tunnel measurements (black) and MERCURE simulations (grey).

To provide an operational model for the effect of street intersections, we have developed a model based on a simplified description of the flow field within a street intersection: the flow in the intersection is imposed by the flow in the connected streets and the flow in the streets is driven by the external atmospheric flow. The model considers the intersection as the junction of street segments and takes into account the mass exchanges at the intersection by means of a balance of the incoming and outgoing fluxes; each street is characterized by an average velocity U_{street}, which depends on the intensity and the direction of the external wind, as well as on the geometrical characteristics of the street – length, width and height. The model assumes two independent transport mechanisms, one related to the mass exchange in the horizontal plane and the other to the mean vertical air motion. In order to evaluate the pollutant transport in the vertical direction, vertical air fluxes within the intersection are computed as the consequence of an imbalance in the incoming and outgoing fluxes within the intersection.

We assume that the flow in each street contributing to an intersection is driven by the wind field above the buildings, and we have developed simple relationships to compute the air flows as a function of wind velocity and direction, and street geometry (Soulhac et al., 2008). The first step is to divide the streets into two classes – the streets in which the flow is towards the intersection, denoted by the index $m = 1, M$ and those in which the flow is away from the intersection, denoted by the index $n = 1, N$. Yamartino and Wiegand (1986) assumed that there would be perfect mixing within the intersection, so that the concentrations in the outgoing flows would be identical. The measurements and computations presented in Section 4 show that this is not necessarily true, and that mixing within the intersection is often rather limited, as has also been observed by Scaperdas and Colvile (1999) and Robins et al. (2002). This means that the concentrations in the outgoing flows will be determined by the contributions from individual incoming streets, and we cannot simply homogenise the incoming concentrations. So the simple model presented here is based on that the computation of a transfer matrix $Q[m, n]$ which gives the mass flux from any incoming street m into any outgoing street n. Before we can compute this matrix we have to consider the possible exchange with the atmosphere, which will occur if there is an imbalance between the incoming and the outgoing fluxes. Indeed, since these fluxes are computed independently, from a consideration of the flux induced in each street by the wind, there is no reason to expect that the fluxes will balance. The flux imbalance Q_i in the intersection i is given by:

$$Q_i = \sum_{m=1}^{m=M} Q_m - \sum_{n=1}^{n=N} Q_n$$

where a positive value for Q_i indicates that there is more flow entering the intersection from the contributing streets than leaving it through the streets, and a negative value for Q_i indicates that the total flow in the streets leaving the intersection exceeds the total flow in the streets entering the intersection. These two cases have to be considered separately.

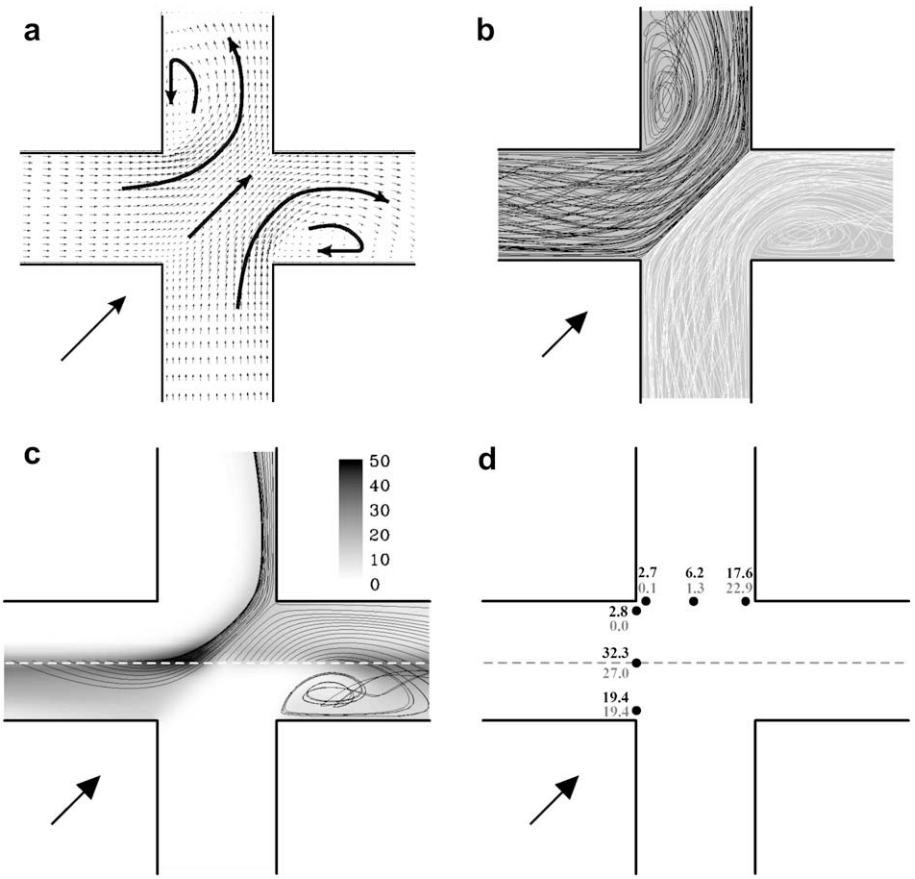

Fig. 10. Flow and dispersion in a street intersection for $\theta = 45^{\circ}$. a) Velocity field at $z = H/2$. b) Streamlines crossing the end of the street no. 1 (black) and streamlines crossing the end of the street no. 2 (white). c) Concentration field C^* on the ground in case of a line source placed in the street no. 2 (MERCURE). d) Concentration values on the ground: comparison between wind tunnel measurements (black) and MERCURE simulations (grey).

5.1. $Q_i > 0$: flow out of the intersection into the atmosphere

The atmosphere acts as a passive sink which receives the excess incoming flux in the intersection. We therefore include the atmosphere as an extra, fictitious, outgoing street $n = N + 1$, and the flux from each of the incoming streets is assumed to contribute to the atmospheric flux in proportion to the flux in that street. The flux to the atmosphere is then given by:

$$Q[m, N+1] = \frac{Q_i}{\sum_{m^*=1}^{m^*=M} Q_{m^*}} Q_m$$

and the modified fluxes entering and leaving the intersection:

$$Q'_m = \left(1 - \frac{Q_i}{\sum_{m^*=1}^{m^*=M} Q_{m^*}}\right) Q_m \quad \textit{fluxes leaving the upwind streets}$$

$$Q'_n = Q_n \quad \textit{fluxes entering the downwind streets}$$

5.2. $Q_i < 0$: flow into the intersection from the atmosphere

The atmosphere acts as a passive source supplying the additional flux required for the outgoing streets, so it is modelled as an additional, fictitious incoming street $m = M + 1$, and the flux from each of the outgoing streets is assumed to receive a contribution from the atmosphere, in proportion to the flux in that street. The flux from the atmosphere is then given by:

$$Q[M+1, n] = \frac{Q_i}{\sum_{n^*=1}^{n^*=N} Q_{n^*}} Q_n$$

and the modified fluxes entering and leaving the intersection become:

$$Q'_m = Q_m$$

$$Q'_n = \left(1 - \frac{Q_i}{\sum_{n^*=1}^{n^*=N} Q_{n^*}}\right) Q_n$$

5.3. The flux transfer matrix

Once the incoming and outgoing fluxes have been modified to include the transfer to or from the atmosphere, the modified fluxes balance:

$$\sum_{m=1}^{m=M} Q'_m = \sum_{n=1}^{n=N} Q'_n$$

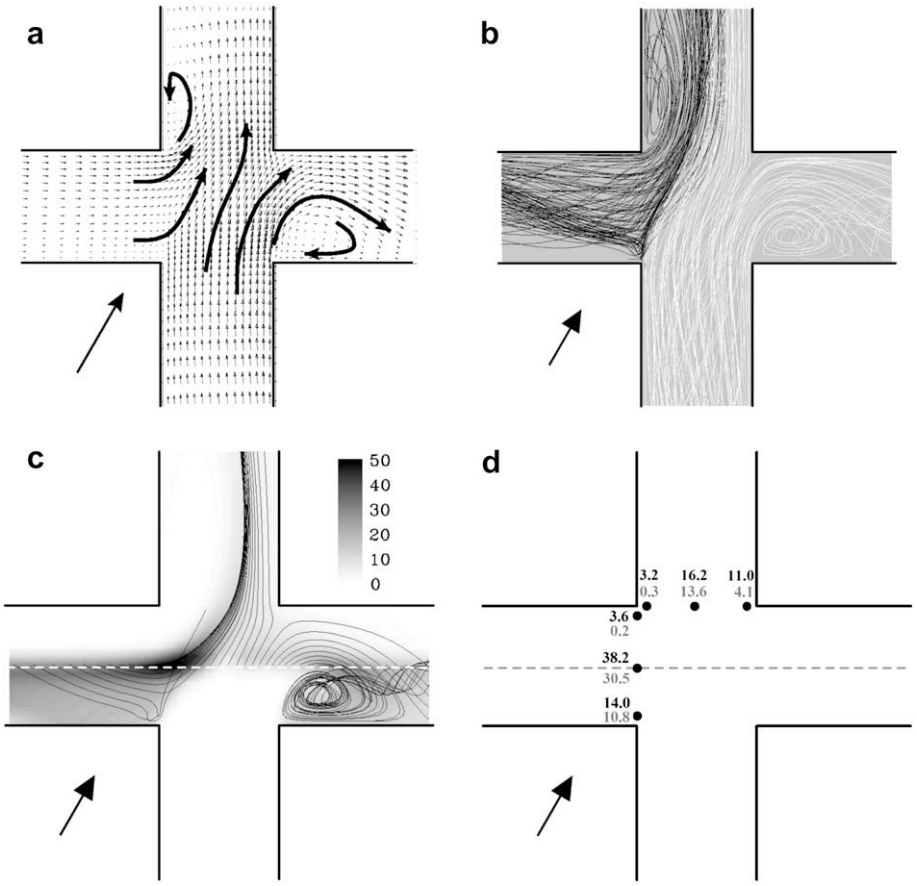

Fig. 11. Flow and dispersion in a street intersection for $\theta = 60°$. a) Velocity field at $z = H/2$. b) Streamlines crossing the end of the street no. 1 (black) and streamlines crossing the end of the street no. 2 (white). c) Concentration field C^* on the ground in case of a line source placed in the street no. 2 (MERCURE). d) Concentration values on the ground: comparison between wind tunnel measurements (black) and MERCURE simulations (grey).

and it only remains to redistribute the incoming fluxes over the outgoing streets.

The model for the advective redistribution of pollutants in the intersection is based on the observation that there is very little vertical variation in the mean flow at any point in the intersection; as can be seen in Figs. 8b–13b, the streamlines hardly cross each other at all. For any given intersection, and set of fluxes within the incoming and outgoing streets, there is only one way in which the incoming fluxes can be redistributed so as to satisfy both the (imposed) outgoing fluxes and the requirement that streamlines must not cross. The method is illustrated with the example shown in Fig. 14; flows Q_1,Q_2 and Q_3 enter through streets 1,2 and 3, and flows Q_4, Q_5 and Q_6 leave through streets 4, 5 and 6. So the streets 1, 2 and 3 correspond to $m = 1, 2, 3$ and the streets 6, 5 and 4 correspond to $n = 1,2,3$ respectively. After the flows have been modified to account for any flux imbalance in the intersection, the fluxes Q_1–Q_6 become Q'_1—Q'_6. Then the transfer matrix $Q[m,n]$ is given by:

$$Q[m,n] = \begin{bmatrix} Q'_6 & Q'_1-Q'_6 & 0 \\ 0 & Q'_2 & 0 \\ 0 & 0 & Q'_3 \end{bmatrix} \quad (4)$$

If there is a flow out of the intersection into the atmosphere, the transfer matrix would be:

$$Q[m,n] = \begin{bmatrix} Q'_6 & Q'_1-Q'_6 & 0 & \alpha Q_1 \\ 0 & Q'_2 & 0 & \alpha Q_2 \\ 0 & 0 & Q'_3 & \alpha Q_3 \end{bmatrix}, \quad where\ \alpha = \frac{Q_i}{\sum_{m=1}^{m=3} Q_m} \quad (5)$$

and if there is a flow from the atmosphere into the intersection it would be:

$$Q[m,n] = \begin{bmatrix} Q'_6 & Q'_1-Q'_6 & 0 \\ 0 & Q'_2 & 0 \\ 0 & 0 & Q'_3 \\ \beta Q_6 & \beta Q_5 & \beta Q_4 \end{bmatrix}, \quad where\ \beta = \frac{Q_i}{\sum_{n=1}^{n=3} Q_n} \quad (6)$$

Once the air fluxes have been computed it is straightforward to compute the pollutant fluxes and the concentrations in the outgoing flows. The flows Q_m in the incoming streets transport pollutant at a concentration C_m, so the pollutant mass flux in each incoming flow is just $Q_m C_m$. For the case in which there is no flux imbalance, and hence no exchange with the overlying atmosphere, the concentrations in the outgoing street n are then just given by:

$$C_n = \sum_{m=1}^{m=M} Q[m,n] C_m / \sum_{m=1}^{m=M+1} Q[m,n]$$

This can readily be extended to cover the two cases involving exchanges with the atmosphere.

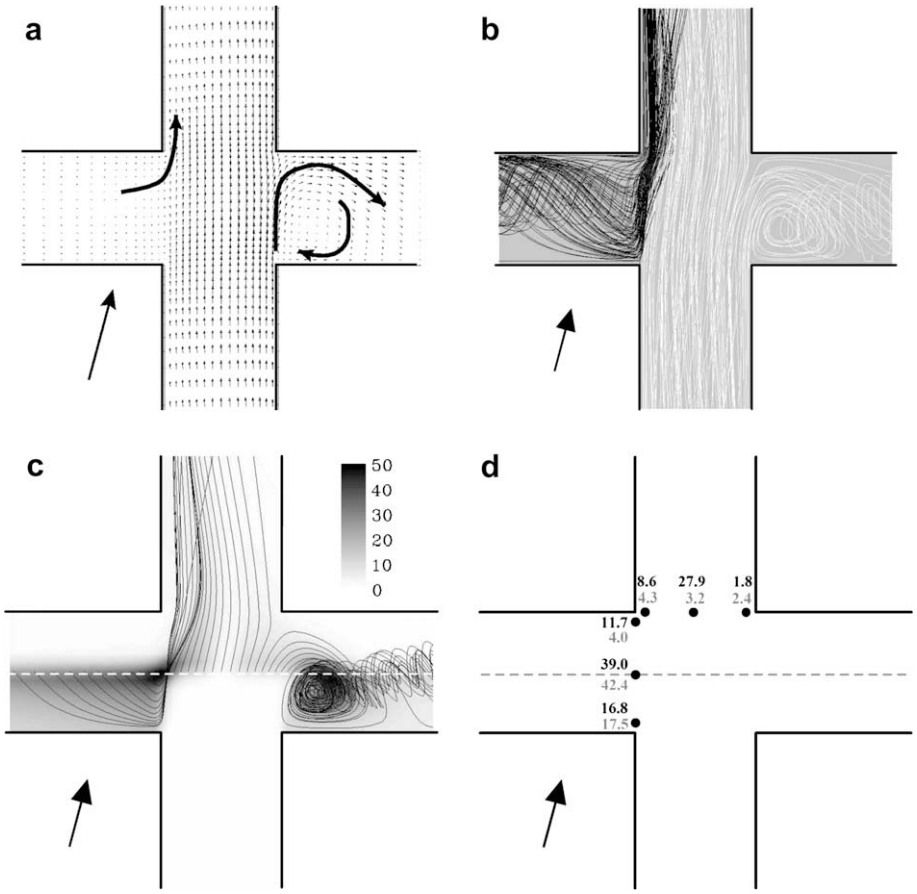

Fig. 12. Flow and dispersion in a street intersection for $\theta = 75°$. a) Velocity field at $z = H/2$. b) Streamlines crossing the end of the street no. 1 (black) and streamlines crossing the end of the street no. 2 (white). c) Concentration field C^* on the ground in case of a line source placed in the street no. 2 (MERCURE). d) Concentration values on the ground: comparison between wind tunnel measurements (black) and MERCURE simulations (grey).

5.3.1. Effect of fluctuations in wind direction

The simple model for convective exchange in the intersection assumes that the wind will be steady over the averaging period, but this is rarely the case, and fluctuations in wind direction can have an important influence on the eventual redistribution of pollutants within the intersection. To model this effect simply, we compute an average transfer matrix $\overline{Q}[m,n]$ for each intersection, where the average is taken over the time step of the model, and includes fluctuations in wind direction on time scales shorter than the time step of the model. In an urban dispersion model, the mass exchanges in each intersection can then be computed using this averaged transfer matrix. We assume that the concentrations depend principally on conditions in the neighbourhood of the intersection, and do not change much over the averaging period for the wind. We also assume that fluctuations in wind speed are uncorrelated with fluctuations in wind directions, so the average flux redistribution in the intersection does not depend on wind speed.

The average transfer matrix is computed assuming that the fluctuations in wind direction θ are small enough that they can be modelled by a Gaussian probability density function:

$$f(\theta) = \frac{1}{\sigma_\theta\sqrt{2\pi}}\exp\left\{-\frac{1}{2}\left(\frac{\theta-\theta_0}{\sigma_\theta}\right)^2\right\} \tag{7}$$

where θ_0 is the mean wind direction during the model time step and σ_θ is the standard deviation of the angle, over that period. Then the average transfer matrix is given by:

$$\overline{Q}(\theta_0) = \int_{\theta_0-3\sigma_\theta}^{\theta_0+3\sigma_\theta} f(\theta-\theta_0)Q(\theta)d\theta \tag{8}$$

The average transfer matrix $\overline{Q}[m,n](\theta_0)$ expresses the *average* air flux circulating from a street towards another. The influence of the fluctuations in wind direction depends strongly on the value of the standard deviation σ_θ of the external wind direction. Blackadar (1997) has proposed a simple expression for this variable, based on the standard deviation of the transverse velocity fluctuations σ_v and the average velocity $\overline{u}$:

$$\sigma_\theta \simeq \frac{\sigma_v}{\overline{u}} \tag{9}$$

where σ_θ is expressed in radians. For operational purposes, σ_v can be evaluated directly from *in situ* sonic anemometer measurements or it can be evaluated indirectly from empirical relations which relate σ_v/u^* to z/L_{MO} and z/δ (Fisher et al., 1998), where δ is the boundary layer height and L_{MO} is the Monin–Obukhov length scale.

The value of σ_θ represents the standard deviation of the wind direction due to 'atmospheric turbulence', i.e. higher frequency fluctuations, and meteorological variability in the atmospheric boundary layer, i.e. lower frequency fluctuations (Stull, 1988).

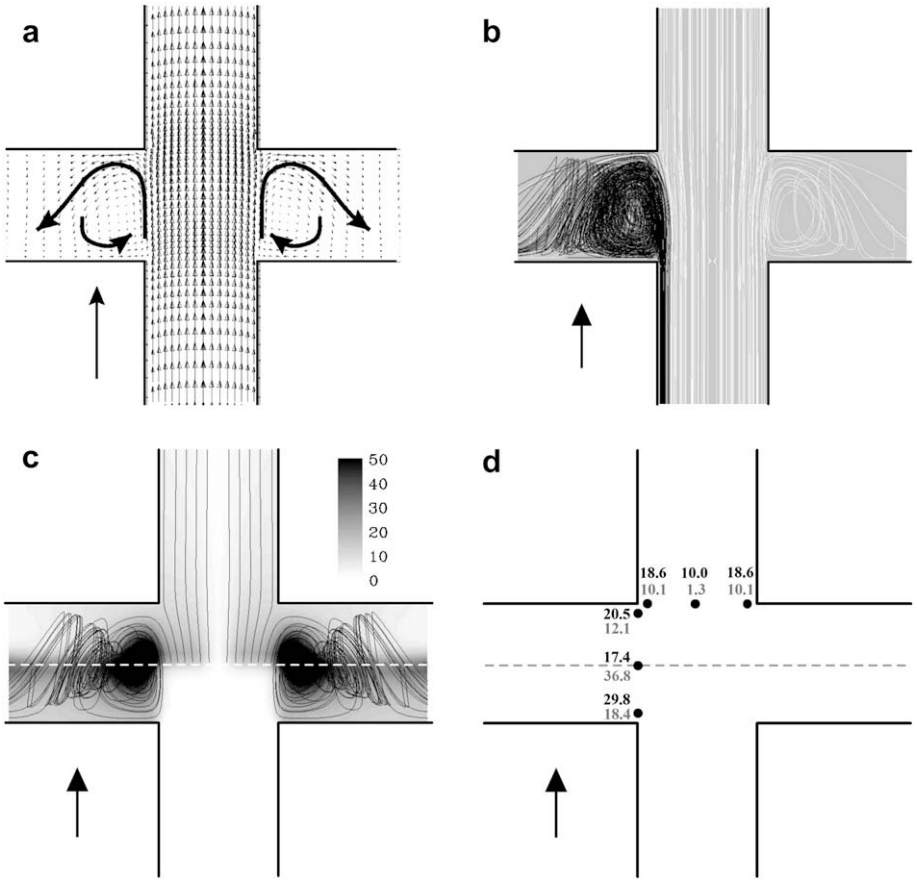

Fig. 13. Flow and dispersion in a street intersection for $\theta = 90°$. a) Velocity field at $z = H/2$. b) Streamlines crossing the end of the street no. 1 (black) and streamlines crossing the end of the street no. 2 (white). c) Concentration field C^* on the ground in case of a line source placed in the street no. 2 (MERCURE). d) Concentration values on the ground: comparison between wind tunnel measurements (black) and MERCURE simulations (grey).

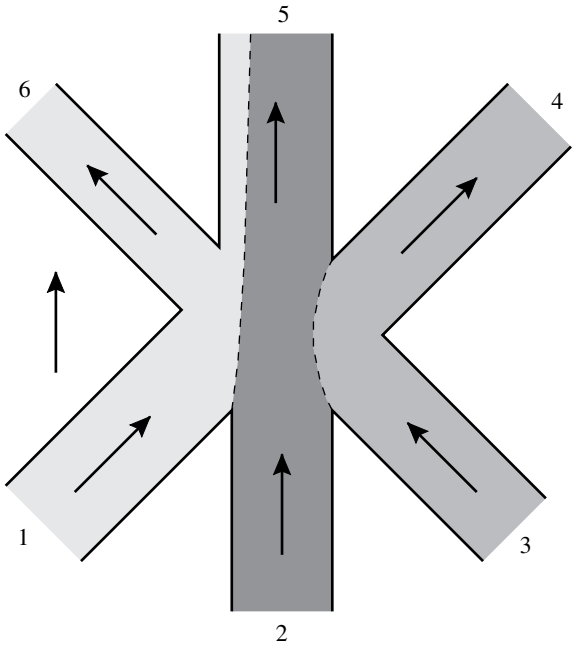

Fig. 14. Internal transport phenomena within the intersection.

6. Conclusion

Flow and dispersion within a street intersection have been studied using numerical and experimental methods. The numerical simulations reproduced some aspects of the wind tunnel experiments well, but other features – most notably the ground-level concentrations away from the axis of the line source – were not captured at all. In the first part of this study we investigated the influence of an intersection on the velocity and concentration fields in the adjoining streets, by comparing conditions within the street with those that occur in an infinitely long street. This showed that the immediate influence of the intersection extends within the adjoining streets, to a distance of the order of the characteristic size of the streets. Flow and dispersion at the entrance to cross-wind streets is dominated by a large vertical-axis recirculating vortex which forms at the interface between the intersection and the street. This vortex also appears to have an important influence on exchanges between the streets and the overlying atmosphere. The intersection also influences the average velocity and the concentration distribution in the street segment between two intersections; for some wind directions the average velocity is the same as that which occurs in an infinitely long street with the same wind, but for other angles the average velocity in the finite-length street is significantly lower. The average concentration along a finite-length street is significantly different from that observed in an infinitely long street.

In the second part of the study we investigated how the pollutant fluxes in the incoming streets are redistributed amongst the outgoing streets. An analysis of the mean streamlines obtained from numerical simulations shows that the flows remain relatively planar, with little variation over the vertical, and we have exploited this result to develop a simple operational model for the redistribution of pollutant fluxes within the intersection. The model also includes exchanges with the overlying atmosphere, computed from a balance of the incoming and outgoing fluxes in the streets. This model has been further adapted to take account of the influence of fluctuations in wind direction over typical averaging periods.

The intersection model is a module of the urban air-quality model SIRANE, which has now been applied to several European cities, including Lyon, Grenoble, Paris, Milan, Turin. Comparisons with field measurements for a number of these cities (Soulhac et al., 2002, 2003, 2004; Boni et al., 2008; Biemmi and Gaveglio, 2007) and with wind tunnel data (Garbero, 2008) enabled us to validate many aspects of the model; these validation studies are the subject of on-going research, and will be described in detail in future publications.

References

Benesh, F., 1978. Carbon Monoxide Hot Spot Guidelines, User's Manual for Interaction-Midblock Model, vol. V. EPA-450/3-78-037.

Biemmi, S., Gaveglio, R., 2007. Dispersione di inquinanti nella città di Milano: parametrizzazione dello strato limite e modellizzazione dei campi di concentrazione. Tesi di Laurea, Politecnico di Torino.

Blackadar, A.K., 1997. Turbulence and Diffusion in the Atmosphere. Springer.

Boni, F., Salizzoni, P., Garbero, V., Genon, G., Soulhac, L., 2008. La modellizzazione dell'inquinamento atmosferico in aree urbane su scala locale: un esempio di applicazione in un quartiere di Torino. GEAM, 124, Anno XLV (2), pp. 63–76.

Bullin, J.A., Hinz, M., Bower, S.C., 1982. Vehicle Emissions from Intersections. Int. Tech. Rep., Texas Transportation Institute. FHWA/SDHPT Project 2250.

Carissimo, B., Dupont, E., Musson-Genon, L., Marchand, O., 1995. Note de principe du code MERCURE version 3.1. Int. Tech. Rep. HE-3395007B. EDF-DER.

Carpentieri, M., 2006. Modelling air quality in urban areas. Ph.D. thesis, Università degli Studi di Firenze.

Dobre, A., Arnold, S., Smalley, R., Boddy, J., Barlow, J., Tomlin, A., Belcher, S.E., 2005. Flow field measurements in the proximity of an urban intersection in London, UK. Atmospheric Environment 39, 4647–4657.

Fisher, B.E.A., Erbrink, J.J., Finardi, S.P., Jeannet, P., Joffre, S., Morselli, M.G., Pechinger, U., Seibert, P., Thomson, D.J. (Eds.), 1998. Harmonisation of the Preprocessing of Meteorological Data for Atmospheric Dispersion Models. European Commission COST Action 710 – Final Report.

Gadilhe, A., Janvier, L., Barnaud, G., 1993. Numerical and experimental modelling of the three-dimensional turbulent wind flow through an urban square. Journal of Wind Engineering and Industrial Aerodynamics 46–47, 755–763.

Garbero, V., 2008. Pollutant dispersion in urban canopy – study of the plume behaviour through an obstacle array. Ph.D. thesis, Politecnico di Torino – Ecole Centrale de Lyon.

Griffin, 1983. An Air Quality Intersection Model. Int. Tech. Rep., FHWA Report No. FHWA-CO-RD-83-14. Colorado Department of Highways, Denver, CO.

Hamlyn, D., Hilderman, T., Britter, R., 2007. A simple network approach to modelling dispersion among large groups of obstacles. Atmospheric Environment 41 (28), 5848–5862.

Hoydysh, W.G., Dabberdt, W.F., 1994. Concentration fields at urban intersections: fluid modeling studies. Atmospheric Environment 28 (11), 1849–1860.

Hoydysh, W.G., Dabberdt, W.F., Schorling, M., Yang, F., Holynskyj, O., 1995. Dispersion modeling at urban intersections. Science of the Total Environment 169, 93–102.

Hunter, L.J., Watson, I.D., Johnson, G.T., 1990. Modelling air flow regimes in urban canyons. Energy and Buildings 15 (3), 315–324.

Kastner-Klain, P., Plate, E., 1998. Windkanalversuche zur verbesserung der ermittlung von kfz-bedingten konzentrationsverteilungen in stadtgebieten. Institut fur Hydrologie und Wasserwirtschaft, Universität Karlsruhe.

Meroney, R.N., Pavageau, M., Rafailidis, S., Schatzmann, M., 1996. Study of line source characteristics for 2-D physical modelling of pollutant dispersion in street canyons. Journal of Wind Engineering and Industrial Aerodynamics 62 (1), 37–56.

Messina, A., 1983. Estimates of Air Pollution Near Signalized Intersections. Int. Tech. Rep., Federal Highway Administration.

O'Toole, D.M., Hilfiker, R.C., Muldoon, G., 1975. Evaluation of Air Quality in the Vicinity of the Intersection of Wisconsin and Western Avenues N.W., Int. Tech. Rep., FHWA Final Report FHWA/DC/OTPP-75/1.

Ott, W.R., 1977. Development of criteria for siting air monitoring stations. Journal of the Air Pollution Control Association 27 (6), 543–547.

Robins, A., Savory, E., Scaperdas, A., Grigoriadis, D., 2002. Spatial variability and source-receptor relations at a street intersection. Water, Air, and Soil Pollution: Focus 2, 381–393.

Rosas, B., Paine, B., Woodruff, J., Halvorson, J., Berka, J., 1980. Measuring and Modeling Carbon Monoxide at a High Volume Intersection. Int. Tech. Rep., Federal Highway Administration and Minnesota Department of Transportation.

Salizzoni, P., Soulhac, L., Mejean, P., Perkins, R.J., 2008. Influence of a two scale roughness on a neutral turbulent boundary layer. Boundary-Layer Meteorology 127 (1), 97–110.

Scaperdas, A., Colvile, R., 1999. Assessing the representativeness of monitoring data from an urban intersection site in central London, UK. Atmospheric Environment 33 (4), 661–674.

Soulhac, L., 2000. Modélisation de la dispersion atmosphérique à l'intérieur de la canopée urbaine. Ph.D. thesis, Ecole Centrale de Lyon.

Soulhac, L., Mejean, P., Perkins, R.J., 2002. Modélisation opérationelle de la pollution atmosphérique à l'échelle d'un quartier d'une agglomeration. Int. Tech. Rep., LMFAF – Ecole Centrale de Lyon.

Soulhac, L., Puel, C., Duclaux, O., Perkins, R., 2003. Simulations of atmospheric pollution in greater Lyon: an example of the use of nested models. Atmospheric Environment 37, 5147–5156.

Soulhac, L., Pradelle, F., Perkins, R.J., 2004. An evaluation of the urban dispersion models SIRANE and ADMS urban using field data from Lyon. In: Suppan, P. (Ed.), Ninth International Conference on Harmonisation within Atmospheric Dispersion Modelling for Regulatory Purpuses Garmish-Partekirchen, Germany.

Soulhac, L., Perkins, R.J., Salizzoni, P., 2008. Flow in a street canyon for any external wind direction. Boundary-Layer Meteorology 126 (3), 365–388.

Stull, R.B., 1988. An Introduction to Boundary Layer Meteorology. Kluwer Academic Publishers, Dordrecht, Netherlands.

Yamartino, R.J., Wiegand, G., 1986. Development and evaluation of simple models for the flow, turbulence and pollutant concentration fields within an urban street canyon. Atmospheric Environment 20 (11), 2137–2156.

Zamurs, J., Piracci, R.J., 1982. Modelling of carbon monoxide hot spots. Journal of the Air Pollution Control Association 32 (9), 947–953.